ASTRONOMY & ASTROPHYSICS
SUPPLEMENT SERIES

Astron. Astrophys. Suppl. Ser. **117,** 261-280 (1996)

Surface photometry of galaxies in low density regions⋆,⋆⋆

J. Vennik[1], U. Hopp[2,4], B. Kovachev[3], B. Kuhn[2] and H. Elsässer[2]

[1] Tartu Observatory, EE2444 Tartu, Estonia, email: vennik@aai.ee
[2] Max-Planck-Institut für Astronomie, Königstuhl, D-69117 Heidelberg, Germany
email: kuhn@mpia-hd.mpg.de
[3] Bulgarian Academy of Sciences, Astronomical Institute, Bul. Zarigradsko Shose 72, 1784 Sofia, Bulgaria
[4] Universitätssternwarte München, Scheiner Str. 1, D-81679 München, Germany
email: hopp@usm.uni-muenchen.de

Received August 17; accepted September 27, 1995

Abstract. — We perform detailed surface photometry, based on B- and/or R-band CCD images of 92 faint galaxies. They are a subsample of those galaxies which were studied by Hopp et al. (1994) in the direction of three nearby voids. We derive integral photometric parameters and radial surface brightness profiles and compare them to those of several faint galaxy samples, located in different environments, and of a bright field galaxy sample. According to the obtained photometric characteristics, our sample is a mixture of intrinsically bright and faint galaxies, about 60% of them belonging to the bright subsample ($M_B \langle -19.0$). These bright ones show mean characteristics of typical Freeman's disks and are mainly located in the background of the observed voids. The faint subsample ($M_B \geq -19.0$) has parameters typical for the low-surface-brightness (LSB) galaxies. There are a few well isolated galaxies both among the bright and faint subsamples. About 40% of studied galaxies reveal ellipticity and position angle variations along of the radius. The $(B-R)$ colour indices of the observed galaxies span over a wide range of 0.5−1.8 mag with a median value at 1.11 mag, rather blue. About 30% of the observed galaxies reveal radial colour gradients at a 5σ significance level. These galaxies show typically red centers and are getting bluer towards the periphery. The most isolated galaxies in our sample show relatively blue colours ($B_T - R_T \simeq 0.8$). About 40% of the studied galaxies have surface brightness profiles which can be described by the model of single exponential disk. 38% of our galaxies have more complicated profiles and either can be approximated by two exponentials or show the presence of a small bulge. 20% of the observed galaxies have central light depression and outer irregularities – typical for some dwarf galaxies. These profile type frequencies are similar to those of faint field galaxy sample. The evolutionary history of both the isolated and clustered galaxies obviously results in similar photometric and structural characteristics. Thus the photometric methods alone are inadequate for selecting galaxies with different isolation properties.

Key words: large scale structure of Universe — galaxies: photometry; fundamental parameters; structure

1. Introduction

Large field observations have demonstrated that (bright) galaxies are predominantly distributed in clusters and groups and/or are arranged into filamentary structures and sheets surrounding huge voids, which are empty of bright galaxies (e.g. Giovanelli & Haynes 1991). It has been demonstrated that the distribution of less luminous galaxies in available redshift catalogs (e.g. the Center for Astrophysics Redshift Survey - CfA, Huchra et al. 1990) is statistically identical to the bright galaxy distribution and follows the morphology-density relation, which is similar to that of bright galaxies (Einasto 1991; Binggeli et al. 1990). The less luminous and dwarfish galaxies (brighter than $M = -15.5$) are slightly more equally distributed. They tend to populate the outer parts of voids and/or define bridges and filaments of faint galaxies, which split large voids into smaller subvoids, but the central parts of the voids still remain empty (Lindner et al. 1995). The question concerning the hypothetic dwarf population in voids, predicted in some theories (e.g. Hoffman et al. 1992) still remains open because the available redshift catalogs are biased against intrinsically faint (and small) galaxies.

A further point of interest is to search for possible differences in structural characteristics between 'void galaxies', if found, and galaxies in the general field, which would cast light into the problems of the

Send offprint requests to: J. Vennik
⋆Partly based on observations obtained at the European Southern observatory, La Silla
⋆⋆Tables 5 to 8 are only available in electronic form at the CDS via anonymous ftp 130.79.128.5

environmental influences on galaxy formation and evolution. As an effect of global environmental influence we consider the well-established morphological segregation of low-surface-brightness dwarf galaxies (LSBDG's) in the Local Supercluster, where gas-poor (elliptical) dwarfs are predominantly concentrated in rich clusters like Virgo and Fornax while gas-rich (irregular) dwarfs are loosely distributed in groups and in general field. This issue is related to the morphology-density relation of giant galaxies (Dressler 1980) and suggests that besides the local conditions the global environment also effects the formation and evolution of dwarf galaxies. A similar effect of morphological segregation in local scales is observed in the Local Group and in other nearby groups of galaxies, where elliptical satellites are more tightly concentrated towards their primaries when compared to the late-type (irregular) satellites (e.g. Einasto et al. 1974).

On the other hand there are still only marginal differences found in structural parameters of galaxies of the same morphology, located in different environments. Karachentseva (1990) found that the HI content of isolated Magellanic irregular dwarf galaxies is significantly higher if compared to the HI content of group members. Zaritsky et al. (1993) noted a weak but significant correlation between the size (but not the Hubble type) of a satellite and the distance from its (late type) primary, as expected, if satellites are tidally truncated. However, the diameters and luminosities of LSBDG's of the same morphology in Virgo cluster are obviously not correlated neither with their Virgo-centric distances (Reaves 1983) nor with local galaxy density (Karachentseva & Vavilova 1995).

In order to tackle similar problems concerning the possible "void population" and the environmental dependence of their characteristics a systematic search for optically faint galaxies was initiated towards selected nearby voids (Hopp 1994). A sample of galaxies of late morphological type, having predominantly low surface brightnesses, was identified in the fields of three nearby voids with velocities ≥ 3500 km s^{-1} (Hopp et al. 1994). For a subsample of 138 galaxies redshifts were measured and converted to distances, which demonstrate that several of these galaxies are very isolated and populate the rims of the voids (Kuhn 1994). The first results of the "void project" are summarized in Hopp et al. (1995). It includes the coordinates of the selected galaxies, their measured redshifts and estimated morphological types as well as first measurements of the basic photometric parameters.

In the present study we will concentrate ourselves onto the detailed surface photometry of a subsample of these galaxies. In Sect. 2 the observations and reductions are described. Section 3 deals with surface photometry algorithm and evaluates the internal consistency of our results. The profile classification and model-fitting is described in Sect. 4. Sample statistics is evaluated and compared to the data for high and normal density samples in Sect. 5. The results are summarized in Sect. 6.

The Hubble constant of $H_0 = 75$ km s^{-1} Mpc^{-1} is used throughout of this paper.

2. Observations and reduction of the frames

Observations

The broad band B and R frames were taken with the Prime focus Focal reducer and CCD camera of the Calar-Alto (CA) 3.5 m telescope during three observing runs in January, March and October 1993. The frames have a scale of $0.53''$ per pixel and a useful field size of about $7'$ in diameter. The exposures were typically 2 min. The seeing was between $1.5-3.0''$ (FWHM). The mean level of the sky background was 21.5 ± 0.2 mag arcsec^{-2} in B and 20.8 ± 0.2 mag arcsec^{-2} in R.

Additional B and R data were obtained with the Prime focus camera and the two-lens-corrector of the CA 3.5 m telescope in September 1992. These frames have a scale of $0.41''$ per pixel and the field size of $7.5' \times 7.5'$. The exposure times were 10 min in B and 5 min in R; the limiting magnitudes of point objects are 24.2 in B and 23.1 in R.

Some further B and R frames were obtained with the EFOSC2 at the 2.2 m telescope on La Silla. More observational details can be found in Hopp et al. (1995).

Reduction and filtering

The raw CCD frames were de-biased and flat-field-corrected as outlined in more detail by Stickel et al. (1993). Then, the frames were searched for cosmic ray hits and possible "hot pixels" by looking for pixel values above the expected noise and checking if they had a point spread function smaller than the estimated seeing. Faulty pixels were replaced by the median value of the surrounding area. A main tool to improve the signal-to-noise ratio is filtering. We applied the adaptive filtering technique described in Lorenz et al. (1993). The main advantage of this technique consists in recognition of the local signal resolution and adapting its own impulse response to this resolution. That means, an adaptive (space variable) filter smooths extensively the background, less extensively the galaxian outskirts and not at all the highest resolution features. Before applying the adaptive filter, bright stars and other galaxies were masked out. This masking is essential for proper determination of the noise statistics used by the filter. The filter size and its strength are variable. Special care must be taken in constructing the mask frame for large filter sizes: the masks for bright objects (stars and galaxies) should be large enough in order to avoid artefacts in outskirts of filtered bright objects.

After the filtering, a careful sky background level determination and subtraction was performed on the smoothed frame, followed by interactively cleaning from

disturbing objects like foreground stars projected onto the galaxy. We applied a polygon editor for this critical procedure.

Photometric calibration

In order to calibrate our images, we observed a number of fields with standard stars in the star clusters M 92, NGC 7790, NGC 2264 and NGC 2419 (Christian et al. 1985). During each night at least two measurements of standard fields were made with both filters at about the same airmasses X at which the galaxy frames were observed. Zero-point magnitudes ($c_{0,i}$), colour coefficients ($c_{1,i}$), and extinction coefficients ($c_{2,i}$) of the form

$$B = b + c_{0,B} + c_{1,B}(b-r) - c_{2,B}X, \quad (1)$$

$$R = r + c_{0,R} + c_{1,R}(b-r) - c_{2,R}X, \quad (2)$$

were fitted to the instrumental data of every observing night, where B, R are standard magnitudes, and b, r are the instrumental magnitudes. The resulting mean coefficients can be found in Table 1 for every observing period.

Table 1. Mean calibration coefficients for different observing runs

Observing run	$c_{0,B}$	$c_{1,B}$	$c_{0,R}$	$c_{1,R}$
Sept.1992	25.01 ± 0.07	0.605	24.74 ± 0.07	0.090
Jan. 1993	24.30 ± 0.04	0.533	23.93 ± 0.02	0.066
Mar. 1993	24.26 ± 0.14	0.570	23.85 ± 0.25	0.038
Oct. 1993	24.84 ± 0.12	0.588	24.51 ± 0.17	0.056

We used the following mean values of the extinction coefficients: $c_{2,B}$= 0.2 and $c_{2,R} = 0.1$. As seen from colour-coefficients $c_{1,B}$ and $c_{1,R}$ in Table 1 the R-system is close to the standard Kron-Cousins system while our B-filter is actually a broad-band BV-filter.

3. Surface photometry algorithm

3.1. *Profile extraction*

The surface brightness profiles of our galaxies were determined by two methods. First, we calculated azimuthally averaged equivalent brightness profiles using the surface photometry routine developed at the Potsdam Astrophysical Institute. This algorithm counts the pixel-intensities in the area between successive isophotes in predefined narrow surface brightness intervals. The differential counts reduced to a unit area, give the azimuthally averaged intensity profile of the galaxy. We plot the profile over the equivalent radius, which is the radius of the circle of the same area as that inside the corresponding (irregular) isophote (de Vaucouleurs et al. 1976). Thus, the first approach reduced the surface photometry essentially to a one-dimensional photometry. Because we are, in this case, summing the pixel intensities of increasing areas this method yields high signal-to-noise ratio for the faint outskirts of the galaxies. The equivalent profile was used to extract the isophotal radii, central surface brightnesses and to determine the best-fitting parameters of the particular luminosity distribution model. In addition to the differential radial surface brightness profile we calculated the growth curve of the galaxy over the equivalent radius by summing the pixel values from the center outwards in successive isophotes. The total magnitude (B_T) was estimated by an asymptotic extrapolation of this radial growth curve. The effective equivalent radius ($r_{\rm eff}$) was read on the growth curve at the half total light and the mean effective surface brightness ($\mu_{\rm eff}$) within $r_{\rm eff}$ was calculated as

$$\mu_{\rm eff} = B_T + 5\log(r_{\rm eff}) + 2.00. \quad (3)$$

The second approach for the surface photometry should recover some information about the two-dimensional structure such as ellipticities and position angles of isophotes. For this purpose we used the ellipse fitting algorithm, which is based on the formulas given in Bender & Möllenhoff (1987) in its realization in the SURFPHOT package running within MIDAS. This method starts the ellipse fitting procedure from the central intensity peak which was determined with a Gaussian momentum analysis for both coordinates. Then, the lower level ellipses were equally spaced in magnitudes and their centers were not fixed, but match the displacement of the centers of the corresponding surface brightness isophotes. The obtained fit was used to construct a smooth galaxy model. Its subtraction from the original image permits us to remove the elliptical component and to detect underlying structures (spiral arms, dust, HII regions).

As a result of the ellipse fitting we obtained a set of radial profiles: surface brightness (SB), minor-to-major axis ratio (b/a), position angle (PA) - both in B and R colours. The surface brightness was calculated as the average surface brightness within an elliptical annulus defined by inner and outer semi-major and semi-minor axes, (a_1, b_1) and (a_2, b_2) respectively. The semi-major axis associated with the average surface brightness of each annulus has been taken as $a = \sqrt{(a_1^2 + a_2^2)/2}$. In some cases the objects are nearly round and then we performed surface photometry with circular apertures. Combining the B and R surface brightness profiles, which were obtained with the one particular set of fitting ellipses applied both to the B and R frames, the colour index profile was constructed.

Figures 9-19 present examples for the obtained profiles. They are selected in order to demonstrate the different profile types (see Sect. 4). Those readers who are interested in obtaining the radial profile sets of all galaxies of this sample should contact the first author.

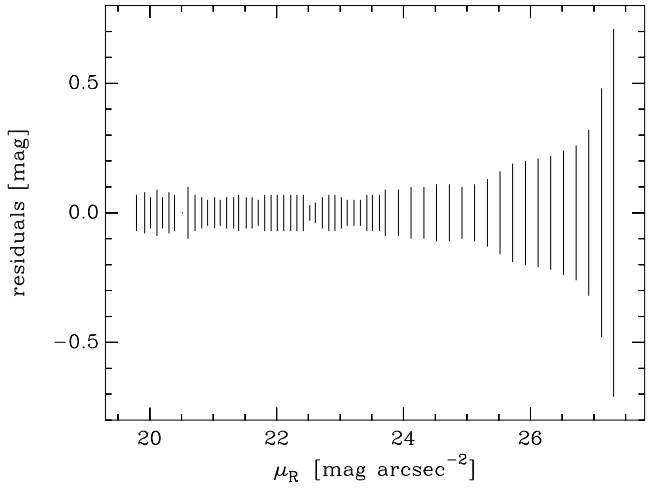

Fig. 1. The 1σ deviations of surface brightnesses of individual R-profiles from their mean values (see text) as function of the surface brightness

Due to the seeing convolution the brightness distribution is flattened near to the center. Therefore the isophotes are rounder and the position angles are uncertain. According to Franx et al. (1989) the effects of seeing can affect these parameters at radii as large as 5 times the seeing FWHM. A further profile "smearing" is caused by the ellipse fitting algorithm itself, because the ellipse centers were not held at a constant position during the fitting process. However this has only limited effects because the studied galaxies have mostly regular shapes without any large irregularities (as bright knots) and real displacements of the ellipse centers for most objects are less than a few arcseconds. The photometric parameters as measured from radial profiles are given in Tables 5 and 6. Table 5 summarizes the data of 82 galaxies, observed in B band, and contains also the $B-R$ colour data of 73 galaxies (9 galaxies where observed only in the B band). Table 6 adds the photometric data of 10 galaxies, which were observed only in the R band. The galaxies are arranged according to the fields and right ascensions as given in Hopp et al. (1995) and data are arranged in tables as follows:

Column 1: The galaxy designation according to Hopp et al. (1995) or the UGC (Nilson 1973) name or the galaxy coordinates, taken from CGCG (Zwicky et al. 1961-68).

Columns 2, 3: The 1950 right ascension and declination, taken from Hopp et al. (1995) or from UGC (Nilson 1973) or from CGCG (Zwicky et al. 1961-68).

Column 4: Asymptotic magnitude.

Column 5: Integrated magnitude within the 25$^{\rm th}$ magnitude isophote.

Columns 6-8: Observed equivalent radius r_{25} (in arcseconds), minor-to-major axis ratio b/a and position angle measured counterclockwise from North PA (in degrees) determined at the 25$^{\rm th}$ magnitude isophote.

Column 9: Observed central surface brightness (in mag arcsec^{-2}).

Column 10: Effective (equivalent) radius (in arcseconds).

Column 11: Colour index extrapolated to the center $(B-R)_0$.

Column 12: Integral colour index $B_T - R_T$.

Column 13: Colour gradient measured on radial colour profile and the 1σ error of the radial colour gradient (in magnitudes per arcsecond).

The absolute magnitudes and reduced effective parameters are given in Tables 7 and 8, which are described in Sect. 4.

Comparing the total asymptotic magnitudes B_T and the integrated magnitudes within the 25$^{\rm th}$ isophote B_{25} as given in Table 5, it is obvious that B_{25} underestimates the total luminosity of our galaxies, normally by about 0.2 mag. In a few cases, the deviations between these two measures increase to 0.9 mag. The large differences appear in galaxies which can be classified as LSB galaxies following the definition by de Blok et al. (1995). These authors found the same effect for their combined sample of LSB galaxies and pointed out that the B_{25}-based luminosities will yield misleading mass-to-light ratios for such galaxies. Therefore, we will use B_T as a good measure of the total luminosity.

3.2. *The internal consistency of the surface brightness data*

The magnitude errors consist of internal and external components. The internal component is dominated by the error of the adopted mean sky value and includes, in addition, the random count error in aperture measurements. In our case the uncertainty in the mean sky value, as measured on filtered CCD frames, is typically less than 0.2% for both the B- and R-frames. Because the typical sky surface brightness is about 21.5 mag arcsec^{-2} in B, our surface brightness profiles are limited to $\mu_B \leq 28$ mag arcsec^{-2}, beyond which limit the error in the mean sky begins to exceed the signal from the object. Following the precept, given by Vader & Chaboyer (1994) (hereafter VC94) we calculated internal errors for surface brightness and colour profiles, which are shown in Figs. 9-19.

We can check the internal consistency of our photometric profiles by performing a simple intercomparison of individual profiles obtained from different frames for the same object in the particular passband. We have two R-frames for VN2#188, VN2#420, VN2#426 and VN2#K117, as well as three R-frames for VN2#274 and VN2#K456. All these frames were processed individually. The mean profile was determined for every particular object and residuals of every single profile from the mean profile were calculated. The 1σ dispersion of these deviations is plotted as error bars over the corresponding surface brightnesses in Fig. 1. The mean error holds about constant at the $\sigma \approx 0.08$ mag level out to the limiting isophote

of $\mu_R = 26.0$ mag arcsec^{-2}, followed by rapid increase at lower surface brightnesses.

The comparison of our total magnitudes with earlier measurements, presented in Hopp et al. (1995), yields following mean residuals: $\langle B_{T,\ \mathrm{our}} - B_{T,\ \mathrm{earlier}}\rangle$=0.05± 0.21 mag and $\langle R_{T,\ \mathrm{our}} - R_{T,\ \mathrm{earlier}}\rangle$=0.02±0.15 mag. Both measurements are based on the same observations and the similarity of results means, that the total magnitudes are not very sensitive to the photometric procedure, applied. We estimate the probable (internal) accuracy of our total magnitudes to be not worse than 0.2 mag in B and 0.15 mag in R.

There are no reliable photometric data available in the literature in order to evaluate the true (external) magnitude transformation errors. The comparison of our blue total magnitudes with those given in Paturel et al. (1989) (hereafter PGC) for 3 galaxies (UGC 8227, PGC 45513 and PGC 45498) in common, yields a poor estimate $B_{T,\ \mathrm{our}} - m_{\mathrm{PGC}} = -0.36\ \pm\ 0.12$ mag. For one more common object (UGC 32) we recognized a large magnitude residual: $B_{T,\ \mathrm{our}} - m_{\mathrm{PGC}} = 1.6$ mag. This galaxy has a very extended low-surface-brightness halo, which strongly contributes to the total magnitude. Its magnitude seems to be overestimated in PGC.

4. Profile fitting and classification

The morphological types estimates of the galaxies are given in Hopp et al. (1995). Here we attempt to quantify the galaxian morphology by means of analyzing their surface brightness profiles. First we provide the profile fitting with a simple analytic function. Upon inspection of our sample of 92 profiles, it becomes evident, that most of them have linear parts (see Figs. 9-18). The obvious next step is to fit the profiles with the exponential intensity law

$$I(r) \ = \ I_0\ \mathrm{e}^{-\alpha r}. \qquad (4)$$

This is the most commonly used model profile for fitting the light distribution of spirals and irregulars, but also for dwarf elliptical galaxies. In surface brightness versus radius it becomes a linear relation:

$$\mu(r) \ = \ \mu_0^{\mathrm{exp}} \ + \ 1.086\alpha r, \qquad (5)$$

with two free parameters: the central surface brightness (μ_0^{exp}) and the exponential scale length ($1/\alpha$). However many observed profiles show a more complex nature: besides of a linear part they exhibit a light excess near to the center (e.g. Figs. 15, 16), indicative of either bulges of early spiral types or nuclei of dwarf ellipticals, or, more often, central light depression (e.g. Figs. 9, 10), typical for many dwarf galaxies or internal flat disk component (e.g. Figs. 17, 18), typical for some giant spirals (Freeman 1970). For classification purposes it is useful to fit a power law as proposed by Sersic (1968)

$$I(r) \ = \ I_0\ \mathrm{dex}(-r^{1/n}), \qquad (6)$$

in which the exponent n is a free parameter. It makes the fitting function more flexible in matching the overall curvature of the observed profiles. As demonstrated by Caon et al. (1993) the involvement of the third parameter is not a pure mathematical tool, but has a certain physical meaning, because n is correlated with global parameters of, at least, early type galaxies. For fitting purposes Caon et al. (1993) suggested the use of the relation

$$\mu(r) \ = \ A + C\ r^{1/n} \qquad (7)$$

For $n = 1$ it coincides with the exponential model, where $C = 1.086\ \alpha$.

We fitted our equivalent light profiles with the power law (7) and determined the best-fitting value of the parameter n. In practice, for each galaxy profile we scanned a grid of values of n ($0.2\ \leq\ n\ \leq\ 30$) and computed the rms scatter of the observed-calculated residuals. We have optimized the value for the exponent by minimizing the rms scatter. The radial range included in this fit spreads from a few arcseconds (to avoid the seeing contribution in the center) to the region where the uncertainty of the sky subtraction renders the light profiles unreliable. In a second attempt the (outer) linear part of every profile has been fitted by pure exponential law ($n = 1$) and the exponential disk model parameters have been determined for most of the observed galaxies, except those few which show nowhere linear parts in their light profiles (e.g. Fig. 19). Power law fitting is straightforward for relatively simple light profiles, which show more or less monotonic curvature over the (linear) radius. Such profiles are inherent for E and S0 galaxies, for many dwarf species and for pure disk galaxies. This method is also useful to describe the light profiles of distant galaxies with their small angular sizes. Here, the central light excess is often smeared out by poor atmospheric seeing.

Our sample contains several cases with more complicated light profiles, which can not be effectively classified by simple power law fitting (Figs. 13, 15-18). For that reason we provide one more (subjective) profile classification.

Several attempts have been done to arrange the light profiles of faint galaxies in a few typical groups. Binggeli & Cameron (1991) (hereafter BC91) allocated the light profiles of the early type dwarfs in Virgo cluster into five types on the basis of relative contributions of the central light excess and the outer exponential component: from type I – showing highest light concentration and being nowhere linear (Fig. 19), through type V – consisting of a single exponential with a pronounced central light depression (Fig. 9). Rönnback & Bergvall (1994) (hereafter RB94) classified the light profiles in their sample of blue LSB galaxies (BLSBG's) by means of the three basic elements: a bulge (b), an exponential disk (d) and a cut-off (c). While BC91 rely upon the reliably measured inner parts of the light profiles only, RB94 record the quite frequent cut-offs in the outer (noisier) parts of the light profiles too.

Our sample is selected among the galaxies of the late morphological types and contains, therefore, only few examples with bright bulges. Thus the classification scheme of RB94 is more suitable for our sample. A further point is that our set of profiles shows many examples with two linear parts, the inner linear section being flatter than the outer component (Figs. 17 & 18). This particular case is similar to the Type II disks of Freeman (1970), however without any visible bulge component. RB94 describe this variety of profiles as dd; in BC91 this type is not represented. We examined both the equivalent profiles and the major-axis profiles and classified them using both the elements of RB94 and the profile types of BC91. We add a new element into the ordinary RB94 notation: halo (h) – an outer extension in the light profile, which may give some hints to the occurrence of an extended halo component, or may be an effect of incorrect background subtraction.

The results of the model-fitting and profile classification are summarized in the second part of the Tables 7 & 8, where data are arranged as follows:
Column 1: The galaxy designation according to Hopp et al. (1995) or the UGC name or the coordinates from CGCG.
Column 2: Distance D (in Mpc) calculated from measured redshifts (Hopp et al. 1995) and corrected to the local rest frame as defined by Nolthenius & White (1987).
Column 3: Absolute magnitude corrected for foreground absorption as determined by Burstein & Heiles (1978).
Column 4: Effective (equivalent) radius $r_{\rm eff}$ (in kiloparsecs).
Column 5: Effective surface brightness $\mu^{\rm c}_{\rm eff}$ corrected for foreground absorption.
Columns 6, 7: Exponential scale length (α^{-1}) in arcseconds and in kiloparsecs, respectively.
Columns 8, 9: Exponential model central surface brightness ($\mu_0^{\rm exp}$) and its corrected value ($\mu_{0,\rm c}^{\rm exp}$), where flattening and foreground absorption corrections are applied according to Freeman (1970).
Column 10: Parameter n of the best fitting power law.
Column 11: Assigned profile type according to RB94.
Column 12: Isolation classes: 1 – in a cluster, 2 – in a sheet, 3 – in outskirts of a sheet, 4 – in a transition region between sheet and void, 5 – in outskirts of a void. 6 – in a void. Distant galaxies with $v_{\rm r} > 12\,000$ km s^{-1} could not be classified (see Sect. 5).

Uncertain entries in tables are designated with a colon.

5. Sample statistics and isolation properties

5.1. *Distribution of the surface photometry parameters*

Here, we evaluate the mean geometric and photometric characteristics of the "void sample" and compare them to bright and faint field galaxy samples.

The distribution of the observed axis ratios $(b/a)_{25}$ at the 25.0 Bmag arcsec^{-2} isophote is shown in Fig. 2. A

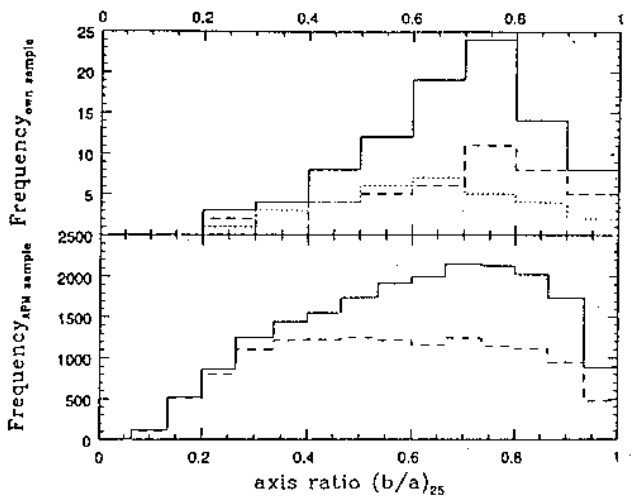

Fig. 2. Distribution of the axis ratios in the presented sample (top). Solid line: complete sample, dashed: only galaxies with $n \leq 1.5$, dotted: only galaxies with $n \leq 1.5$ and $M_B \geq -19.1$; see text for details. The subsample represented by the dotted line is identified with late morphological type dwarfish galaxies. For comparison, the distribution of the APM galaxies according to Lambas et al. (1992) is shown (bottom). Solid line: all, dashed: spirals

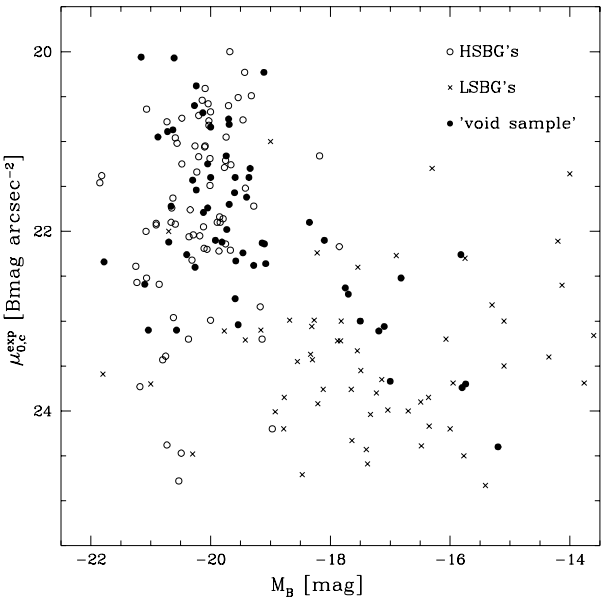

Fig. 3. Relation between the face-on central surface brightnesses of the exponential model and the absolute B-magnitudes for studied galaxies (filled circles) compared to the bright field disk galaxies (open circles) and to the LSB field galaxies (crosses)

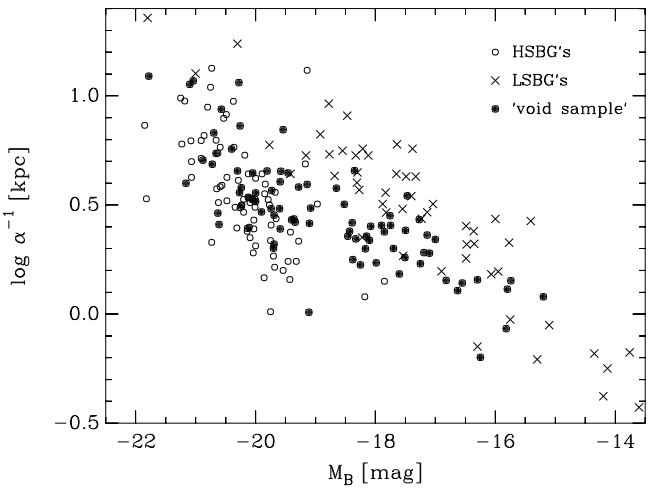

Fig. 4. Relation between the exponential scale lengthes and absolute B-magnitudes of studied galaxies (filled circles) compared to the bright field disk galaxies (open circles) and LSB field galaxies (crosses)

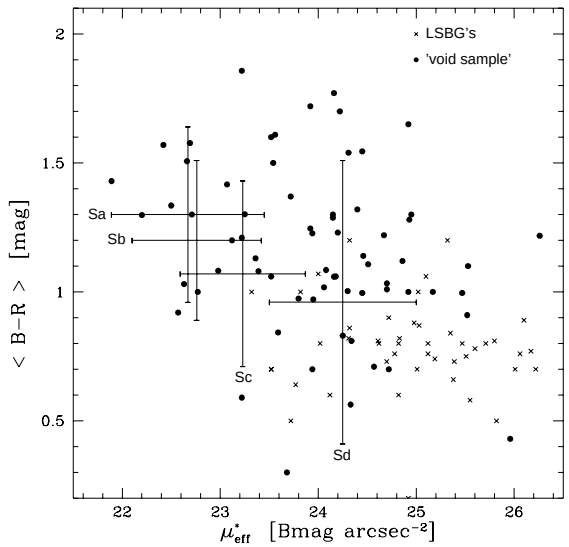

Fig. 5. Relation between the mean colour indices $\langle B-R\rangle$ and the effective surface brightnesses $\mu^*_{\rm eff}$ for studied galaxies (filled dots) compared to the mean colours of the ESO-LV spiral galaxies of different morphological type (large crosses, length indicates the 1-*sigma* width of a gaussian distribution), and LSB field galaxies (crosses, references see text)

simple comparison to the distributions of the APM galaxies by Lambas et al. (1992), who split their large sample according to the morphological type, indicates that our sample should be a mixture of late type and early type galaxies. Further, as shown by Binggeli & Popescu (1995), the ellipticity distribution of galaxies seems to depend on the luminosity too, at least for the Virgo cluster galaxies. We therefore split our sample in those galaxies where the exponential law is a good overall description ($n \leq 1.5$, see above for the definition of n) and those which are more likely described by the de Vaucouleurs' law ($n \geq 1.6$). We identify these two samples with late type and early type galaxies. The early type sample shows a distribution peaked around $b/a \sim 0.73$ while late type galaxies follow a significantly broader distribution, but are still centered around $b/a \sim 0.7$. We further divided the late type sample into a bright ($M_B \leq -19.0$) and a faint ($M_B \geq -19.1$) subsample. The faint subsample has a very broad distribution without a pronounced peak. Its mean value is $b/a = 0.63$ and it includes values from 0.27 to 1.0. The bright sample is a little narrower, it has a pronounced peak at $b/a \sim 0.75$ and a mean value of 0.69. This is a trend similar to the late type dwarfs and spirals of the Virgo cluster (Binggeli & Popescu 1995). A Kolmogoroff-Smirnov test reveals that the distributions of the faint and bright galaxies are significantly different.

Besides of measuring the axes ratios and position angles around the $25^{\rm th}$ magnitude isophote we searched for systematic changes in the radial profiles of both these parameters within the Holmberg radius at $\mu_B = 26.5$ mag arcsec^{-2} excluding the very center within a few arcseconds, which is affected by atmospheric seeing. About 40% of the observed galaxies show axes-ratio-changes and isophote twists, significant at the 3σ level. The isophotes are mostly getting flatter in outer regions. This tendency is more pronounced for nearly exponential light distributions ($0.9 \leq n \leq 1.2$). The isophote twisting is slightly more frequent among galaxies with central light depression ($n \langle 0.9$).

In the Figs. 3 and 4 the central surface brightnesses of the exponential models and exponential scale lengthes of the studied galaxies are plotted over their absolute B-magnitudes (filled circles) and compared to those distributions of the bright spirals, studied by Kent (1985) (open circles), and those of the LSB field galaxies, compiled from several literature sources: de Blok et al. (1995), Karachentseva et al. (1995), McGaugh et al. (1994), Roukema & Peterson (1995), Rönnback & Bergvall (1994). The R-magnitudes of Kent (1985) are converted to the B-magnitudes applying the mean colours $B-R = 1.3$ for S0-types and $B-R = 0.9$ for other spiral and irregular types, as given in Kent (1984). The distance-dependent parameters are reduced to $H_0 = 75$ km s^{-1} Mpc^{-1}. As shown in the Figs. 3 and 4 the studied galaxies span over a large luminosity range and sample both the bright and

faint (field) galaxies. We can arbitrarily divide the studied galaxies into subsamples of bright ($M_B\langle -19.0$) and faint ($M_B \geq -19.0$) galaxies, applying $M_B \approx -19$ as an approximate limiting magnitude of the Kent's sample of bright field disk galaxies. The mean parameters of the "void sample" are compared to the parameters of two field samples in Table 2.

The parameters of the galaxies in our bright subsample accord with those of the bright disk galaxies and show the central surface brightnesses of the typical Freeman's disks. Our faint subsample consists of slightly brighter (and smaller) galaxies if compared to the typical LSB field galaxies. As seen in Fig. 4 the sizes of LSB disks overlap those of HSB disks and, remarkably, the LSB disks being more extended than HSB disks of the same total luminosity. The total spread in $\log(\alpha^{-1})$ off all three samples taken together is nearly a factor of two larger at the bright end than at the faint one. This surely reflects a selection effect inherent to all three samples. Intrinsically small and faint galaxies are difficult to find with the methods applied here, but this can be overcome at least for star forming dwarfs by searches for emission line galaxies (Hopp & Kuhn 1995).

We calculated three different $B-R$ colour indices: the colour index extrapolated to the center $(B-R)_0$; total (luminosity weighted) colour index ($B_T - R_T$) and the area weighted colour index $\langle B-R\rangle$. The last parameter was determined by averaging the colour profile out to about the Holmberg radius excluding the very center within a few arcseconds. These two total color indices may differ for galaxies with bright (usually red) central bulges. For the present sample the luminosity weighted and the area weighted colour indices show zero-mean-difference with 1σ dispersion of 0.11 mag. The colour and surface brightness characteristics of the studied galaxies are compared to those of normal HSB and LSB field galaxies in Fig. 5. The data for HSB galaxies are obtained from de Blok (1995), who sampled the spiral galaxies in the Surface Photometry Catalogue of the ESO-Uppsala Galaxies (Lauberts & Valentijn 1989, hereinafter ESO-LV), and binned them according to their morphological types. The corresponding mean values and 1σ deviations for Sa, Sb, Sc and Sd galaxies are plotted in Fig. 5 against the effective surface brightness ($\mu^*_{\rm eff}$), measured at the effective radius. We note the different definitions of the effective SB in the ESO-LV and in the present work (expression 3). For comparison purposes we calculated $\mu^*_{\rm eff}$ for our sample in a simple way, applying the disk-model parameters, as described by de Blok et al. (1995). The data for the LSB field galaxies are compiled from several literature sources: de Blok et al. (1995), McGaugh et al. (1994) and Roukema & Peterson (1995). The $B-V$ colour indices of McGaugh et al. (1995) were transformed to the $B-R$ indices by means of the empirical relation in ESO-LV: $B-R = 1.5\,(B-V) + 0.1$, (RB94). The colours of the studied galaxies are similar to the colours of normal field galaxies. Both samples show a large scatter. The reddest colours among the studied galaxies ($B-R > 1.6$) are measured mostly for distant galaxies with $0.07 \leq z \leq 0.2$. The colours of these probably late type and distant galaxies are reddened up to 0.4 mag through the K-effect (Rocca-Volmerange & Guiderdoni 1988). We do not correct our data for the K-effect because the morphological types of the studied galaxies are poorly known. The mean colours with 1σ deviations are compared in Table 2, where the estimate for HSB galaxies is obtained from RB94 (their Fig. 1).

5.2. *Photometric properties and environment*

Our basic aim was to search for very isolated galaxies and compare their photometric parameters to those of clustered galaxies. Earlier analysis of the measured redshifts has revealed that the initial "void sample", though being a low density sample, contains some clustered objects too (Hopp et al. 1995). Next we attempt to evaluate the true isolation of individual galaxies in our subsample and compare the characteristics of galaxies belonging to different isolation classes. Kuhn (1994) analyzed the isolation of the galaxies in the "void sample" by comparing their distribution to that of CfA-sample and calculated for every particular galaxy the distance to its nearest neighbour. Because the CfA-sample is apparent magnitude limited the derived nearest-neighbour distances are not directly comparable at different redshifts. We attempted to evaluate the true isolation by means of analyzing the cone diagrams in addition to the calculated nearest-neighbour distances.

In effect we divided the galaxies into isolation classes as described at the end of Sect. 4 and listed in Tables 7 and 8 (Col. 13). There are 43 out of 92 galaxies in our sample within the given redshift limit; 11 galaxies of them are related to (small) clusters (isolation class 1); 23 of them are related to sheets delineating the voids (classes 2 & 3). Only 9 galaxies are well isolated, mostly populating the outskirts of the nearby voids (classes 4 – 6). The photometric characteristics of the galaxies belonging to different isolation classes are compared in Fig. 6.

We notice the differencies between the distributions of distant and nearby ($v_{\rm r}\langle$ 12 000 km s^{-1}) galaxies, the first being systematically of lower surface brightnesses and larger sizes. This can be explained with our selection criteria and several observational biases. As seen in Figs. 3 & 4 the intrinsic scatter of the exponential scale parameters among the HSB and LSB disk galaxies is large, even larger than in our studied sample. According to the search strategy (Hopp 1994) we selected as high priority void-galaxy-candidates the large sized objects of diffuse appearance. That means the distant galaxies should be biased toward larger sizes and lower SB's. Some observational biases can also contribute to the scatter in Fig. 6 at higher luminosities. For small angular size distant galaxies the

Table 2. Mean photometric characteristics of the 'void sample' and two field samples

Parameter	Present study			HSB	LSB
	$M_B\langle -19.0$	$M_B \geq -19.0$	Total	disk galaxies	galaxies
$N_{\rm gal}$	53	39	92	74	61
M_B (mag)	-20.1±0.6	-17.5±0.9	-18.9± 1.4	-20.2±0.7	-17.2±1.9
$\mu_{0,c}^{\rm exp}$ (Bmag arcsec^{-2})	21.7±1.0	22.7±0.6	22.1±1.0	21.8±1.1	23.3±0.9
α^{-1} (kpc)	4.6±2.7	2.1±0.8	3.4±2.4	4.3±2.7	3.9±4.0
$\langle B-R\rangle$ (mag)	1.31±0.32	1.02±0.29	1.20±0.33	1.27	0.79±0.20

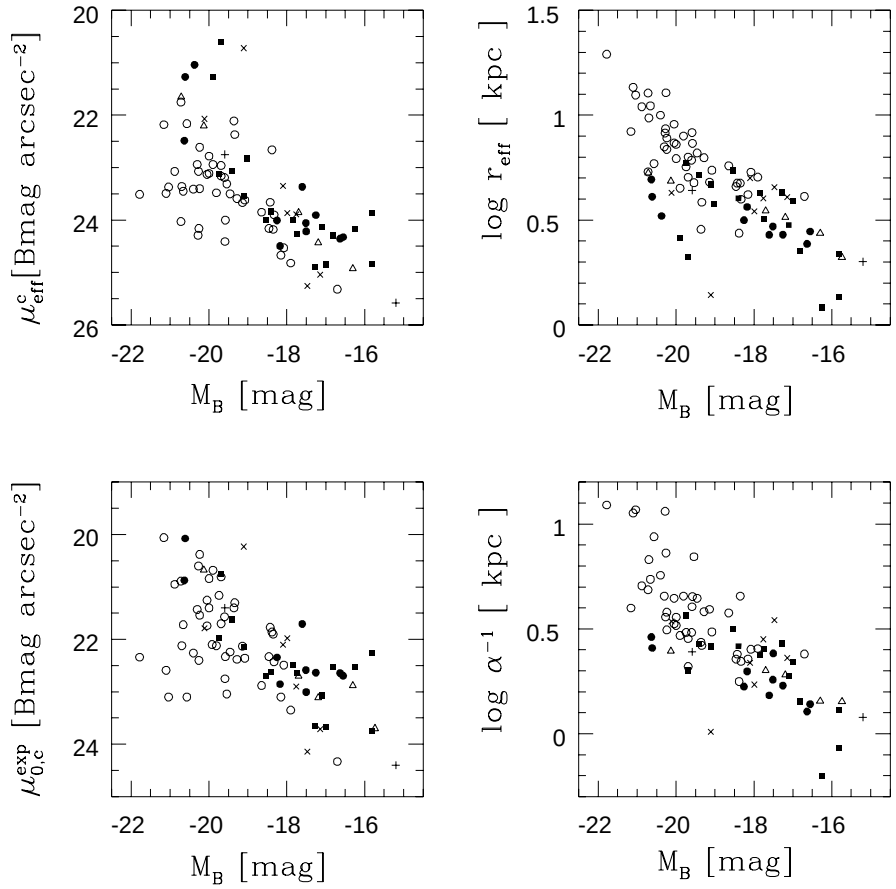

Fig. 6. Relations between the surface brightness characteristics: **a)** effective face-on surface brightness, **b)** log effective radius, **c)** central face-on surface brightness of the exponential model, **d)** exponential scale length and the absolute B-magnitude. Galaxies are coded according to their isolation classes as follows: cluster members - filled hexagons; galaxies in a sheet - filled rectangles; galaxies in outskirts of sheets - triangles; galaxies in the transition region between sheet and void - plus signs (+); galaxies in voids and in outskirts of voids - crosses (×); galaxies in the background - small circles

central light excess is smeared out by atmospheric seeing, resulting in lower central surface brightnesses (and probably in larger scale lengthes). For the most distant galaxies ($z \simeq 0.2$) the cosmological SB-dimming, which is proportional to $(1+z)^4$ and the K-effect contribute to the scatter of observed surface brightnesses as well as to systematic shifts towards fainter SBs. On the other side the relatively small scatter among the (absolutely) faint subsample is obviously due to our detection limit at about $\mu_{\rm eff}^{\rm c} \simeq 25.5$ Bmag arcsec^{-2}. Figure 6 does not reveal any significant differences between the clustered and isolated galaxies, probably due to poor statistics. All isolation classes are about equally represented among the bright and faint subsamples. The most isolated galaxies are not necessarily

low luminosity objects, as often assumed. *There are a few luminous and HSB isolated galaxies too.* We note the tight correlation between the size parameters of clustered galaxies and their luminosities in Fig. 6. The sheet members and isolated galaxies scatter much more in these plots. Available data are insufficient in order to distinguish between the effective parameters and the disk scale parameters of galaxies, belonging to different isolation classes in more detail. However isolated galaxies could probably be distinguished by their colour characteristics.

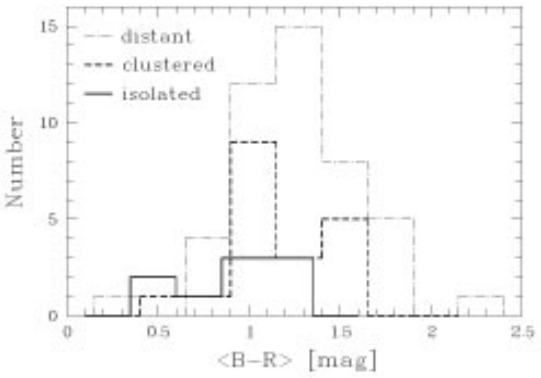

Fig. 7. The frequency distribution of the observed area weighted colour indices $\langle B-R\rangle$ for three different isolation groups: isolated galaxies - thick continuous line, clustered galaxies - thick dotted line, distant (background) galaxies - thin continuous line

Table 3. $B-R$ colour indices of studied galaxies

Isol. class	$N_{\rm gal}$	$(B-R)_0$ (mag)	B_T-R_T (mag)	$\langle B-R\rangle$ (mag)
bkg	47	1.63±0.41	1.24±0.27	1.27±0.34
1	10	1.52±0.21	1.35±0.21	1.30±0.21
2	9	1.33±0.30	1.00±0.43	1.02±0.26
3	4	1.44±0.55	1.03±0.18	1.13±0.18
4&5&6	5	1.08±0.14	0.77±0.19	0.76±0.30

We divided the studied sample into three groups: background (bkg) galaxies, clustered galaxies (isolation classes 1, 2) and "isolated" galaxies - combining the isolation classes 3 through 6, in order to improve the statistics for the latter group. We compare the frequencies of the area-weighted colors of these three groups in Fig. 7. According to the Kolmogorov-Smirnov test only the distributions of background and isolated galaxies are significantly different (with probability of 0.046 that these two distributions issue from the same parent distribution). A more detailed comparison of the mean colours of galaxies in different isolation classes is given in Table 3. The five most isolated galaxies for which colours are available, are considerably

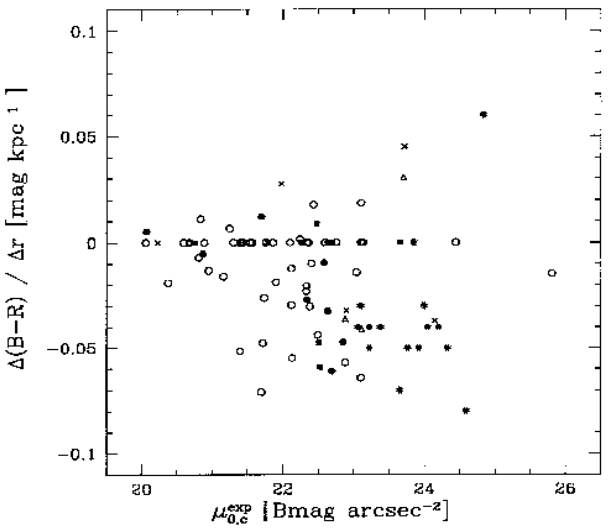

Fig. 8. The relation between colour gradients (in magnitudes per kiloparsec) and the disk model face-on central surface brightnesses. Different isolation classes are coded as in Fig. 6. The data for LSB galaxies of de Blok et al. (1995) are shown, for comparison, by asterisks

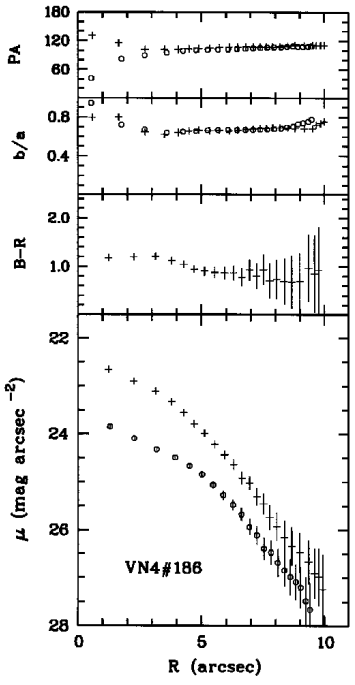

Fig. 9. Light distribution in the galaxy VN4#186. Semi-major axis profiles of surface brightness, $B-R$ colour index, axis ratio b/a, major-axis position angle (PA, 0 on positive x-axis, increasing to positive y-axis). Circles indicate data from B-passband, crosses – from R-passband. The B and R light profiles are both classified as type **cd** in RB94 notation and as type V according to BC91 (see Sect. 4)

bluer when compared to the mean colours of clustered and distant galaxies.

About a third of studied galaxies show colour changes within the given radial interval. In Fig. 8 the measured colour gradients are plotted against the disk central SB, while different isolation classes are coded as in Fig. 6. Among studied galaxies the luminous Freeman's disks with $\mu_{0,c}^{\rm exp} \leq 21.65$ Bmag arcsec^{-2} do not reveal any significant colour changes, indicating rather homogeneous disk stellar content. For the lower luminosity disks the negative colour gradients are dominating. That means, these galaxies have mostly red centers and are getting bluer towards their periphery. The question concerning the colour gradients is intriguing because, if real, they may give information about different stellar populations and about star formation histories, which may be specific in low density environments. It may be indicative that among the four most isolated galaxies two of them show clearly positive colour gradients (have blue centers), which is opposite to the main bulk of observed galaxies.

Recently de Blok et al. (1995) performed a multicolour surface photometry of 21 LSB galaxies. For 16 studied galaxies they determined colour profiles. All but one studied LSB galaxy reveal negative $B-R$ colour gradients. The data from de Blok et al. (1995) are compared to our results in Fig. 8 (asterisks). The tendency toward negative gradients is more pronounced for LSB galaxies. The isolation properties of these LSB galaxies are not yet known, but they obviously do not reside in dense regions.

Besides the comparison of standard photometric parameters we attempt to quantify the profile-type frequencies in different environments. In order to improve the poor statistics of isolated galaxies we again disentangle only between three different isolation classes: clustered galaxies, isolated galaxies and background (not classified) galaxies. The corresponding profile type frequencies are summarized in Table 4. For comparison with our results we classified in a similar manner some sets of SB-profiles, available in the literature and representing different environments. As an example of the faint LSB galaxies in general field we combine the profiles from de Blok et al. (1995), Karachentseva et al. (1995), McGaugh et al. (1994), Rönnback & Bergvall (1994) and Roukema & Peterson (1995). A sample of satellite galaxies, studied by Vader & Chaboyer (1994) around of bright Shapley-Ames galaxies, represents the environment of loose groups. The cluster environment is represented by the extensive studies of Virgo cluster dwarf galaxies in Binggeli & Cameron (1991, 1993). From the latter study we obtain only the data for S0 and later morphological types in order to match the the morphological composition of the present study and of other comparison samples. All samples included in Table 4 are certainly incomplete and the presented comparison is to be treated as a very approximate one.

The profile-type frequencies of the studied galaxies concord with those of the LSB field galaxies. Both samples show higher percentage of single exponential profiles and less multicomponental profiles with central light excess (type bd in RB94 notation and types II & III by BC91), if compared to the satellite galaxies and non-elliptical Virgo dwarfs. The lower percentage of prominent bulges among studied galaxies is probably due to the selection of the void-galaxy-candidates among late type galaxies of diffuse appearance. A few ellipticals have been observed as backup objects and were not regarded as probable "void galaxies" (Hopp et al. 1995). However the distribution of profile-type frequencies among of studied galaxies shows, that galaxies with central light excesses are rather numerous in the subgroup of relatively isolated galaxies.

6. Summary of results

This photometric study demonstrated that the total magnitudes and surface brightnesses of observed 'void galaxies' span over wide ranges: $-15.0 > M_B > -21.5$ mag and $24.5 > \mu_{0,c}^{\rm exp} > 20$ Bmag arcsec^{-2}, respectively. The distribution of basic photometric parameters in our sample corresponds to the similar distributions of field galaxies. Hence the studied galaxies correspond to a mixture of bright and faint field galaxies. About 60% of them belong to the bright subsample ($M_B \langle\ -19.0$), which shows the mean parameters of typical Freeman's disks. The mean parameters of the faint subsample ($M_B \geq -19.0$) correspond to those of brightest LSB field galaxies. About a third of the studied galaxies show radial colour gradients, indicating some changes in stellar populations along the radius. Typically the centers are redder than the outer parts. About 40% of galaxies show ellipticity and position angle variations along the radius.

About half of the studied galaxies are distant objects projecting onto the area of the nearby voids. Their isolation properties are not yet known. Most of the nearby galaxies belong to clusters or sheets, which outline the voids. Only 9 out of 92 studied galaxies populate the voids or outskirts of voids. The most isolated galaxies are not necessarily intrinsically faint, but they have blue colours. The studied sample is dominated by disk galaxies. The profile-type frequencies resemble those of the LSB field galaxies.

The results show that it is difficult to select possible void members by photometric or morphological criteria as objects with the same properties are also common among sheet and even cluster members. To study whether or not true void galaxies deviate somehow in their intrinsic shape from those objects in higher galaxy density region, one needs a larger sample of isolated candidates. Several surveys are presently done to find these galaxies. In a future paper, we will study the emission line galaxies searched by us towards the same voids (see Popescu et al. 1994) with the methods presented here.

Table 4. Comparison of the light profile type frequencies in different galaxy density regions

Profile description	Profile type		Present study total (bkg/cl/isol) %	LSB galaxies (field) %	Satellite galaxies VC94 (groups) %	Virgo dwarfs BC93 (cluster) %
	RB94	BC91				
Non-exponentials	-	I	3(2/4/6)		12	2
Inner excess + outer disk	bd	II, IIIa,b	25(18/28/37)	24		48
Inner (flat) "disk" + outer disk	dd	-	13(14/16/6)	10	64	3
Single exponential	d, dc	IVa,b	40(45/36/31)	41	10	25
Central depression and outer irregularities	cd, cc	V	19(20/16/19)	25	14	22
Number of studied galaxies			92(49/25/16)	70	82	114

Acknowledgements. We acknowledge the support by Dr. G.M. Richter for using his software package and Dr. P. Vader for making available a set of SB-profiles of the satellite galaxies. J.V. gratefully acknowledge the financial support and hospitality of the Max-Planck-Institute for Astronomy during several visits. B. Kov thanks the Alexander von Humboldt Foundation and the DFG for financial support.

References

Bender R., Möllenhoff C., 1987, A&A 177, 71
Binggeli B., Tarenghi M., Sandage A., 1990, A&A 228, 42
Binggeli B., Cameron L.M., 1991, A&A 252, 27 (BC91)
Binggeli B., Cameron L.M., 1993, A&AS 98, 297 (BC93)
Binggeli B., Popescu C.C., 1995, A&A 298, 63
Burstein D., Heiles C., 1978, ApJ 225, 40
Caon N., Capaccioli M., D'Onofrio M., 1993, MNRAS 265, 1013
Christian C.A., Adams M., Barnes J.V., Butcher H., Mould J.R., Siegel M., 1985, PASP 97, 363
de Blok W.J.G., van der Hulst J.M., Bothun G.D., 1995, MNRAS 274, 235
de Vaucouleurs G., de Vaucouleurs A., Corwin H.G., 1976, Second Reference Catalogue of Bright Galaxies. Austin Univ. of Texas Press (RC2)
Dressler A., 1980, ApJ 236, 351
Einasto J., Saar E., Kaasik A., Chernin A.D., 1974, Nat 252, 111
Einasto M., 1991, MNRAS 252, 261
Ferguson H.C., Sandage A., 1991, AJ 101, 765
Franx M., Illingworth G.,Heckman T., 1989, AJ 98, 538
Freeman K.C., 1970, ApJ 160, 811
Giovanelly R., Haynes M.P., 1991, ARA&A 29, 499
Hoffman Y., Silk J., Wyse R.F.G., 1992, ApJ 388, L13
Hopp U., 1994, "Dwarf Galaxies". In: Meylan G., Prugniel P. (eds.), ESO Conference and Workshop Proc. 49, 37
Hopp U., Kuhn B., Elsässer H., Birkle K., Thiele U., 1994, "Astronomy from Wide-Field Imaging". In: MacGillivray H.T. et al. (eds.), Proc. IAU Symp. 161, 705
Hopp U., Kuhn B., Thiele U., Birkle K., Elsässer H., 1995, A&AS 109, 537
Huchra J.P., Geller M.J., de Lapparent V., Corwin H.G., 1990, ApJS 72, 433
Impey C., Bothun G., Malin D., 1988, AJ 330, 634
Karachentseva V.E., 1990, Pis'ma Astron. Zh. 16, 99
Karachentseva V.E., Vavilova I.B., 1995, "Kinematika i fizika nebesnych tel" (in press)
Karachentseva V.E., Prugniel Ph., Vennik J., Richter G.M., Thuan T.X., Martin J.M., 1996, A&AS (in press)
Kent S.M., 1985, ApJS 56, 105
Kent S.M., 1985, ApJS 59, 115
Kuhn B., 1994, Thesis Uni. Heidelberg
Lambas D.G., Maddox S.J., Loveday J., 1992, MNRAS 258, 404
Lindner U., Einasto J., Einasto M., Freudling W., Fricke K., Tago E., 1995, A&A (in press)
Lorenz H., Richter G.M., Capaccioli M., Longo G., 1993, A&A 277, 321
McGaugh S.S., Bothun G.D., 1994, AJ 107, 530
Nilson P., 1973, Uppsala General Catalogue of Galaxies, Uppsala Obs. Ann. 6 (UGC)
Nolthenius R., White S.D.M., 1987, MNRAS 225, 505
Paturel G., Fouqué P., Bottinelli L., Gouguenheim L., 1989, Catalogue of Principal Galaxies, Lyon (PGC)

Popescu C.C., Hopp U., Hagen H., Elsässer H., 1994, Astron. Ges. Abstract Ser. 10, 104
Reaves G., 1983, "Star-forming dwarf galaxies and related objects". In: Knuth D. et al. (eds.). Edition Frontiers
Rocca-Volmerange B., Guiderdoni B., 1988, A&AS 75, 93
Roukema B.F., Peterson B.A., 1995, A&AS 109, 511
Rönnback J., Bergvall N., 1994, A&AS 108, 193 (RB94)
Sersic J.-L., 1968. Atlas de galaxias australes. Observatorio Astronomico, Cordoba
Stickel M., Fried J.W., Kúhr H., 1993, A&AS 98, 393
Vader J.P., Sandage A., 1991, ApJ 379, L1
Vader J.P., Chaboyer B., 1994, AJ 108, 1209 (VC94)
Zaritsky D., Smith R., Frenk C.S., White S.D.M., 1993, ApJ 405, 464
Zwicky F., Wild P., Herzog E., Karpowicz M., Kowal C., 1961-68, Catalogue of Galaxies and Clusters of Galaxies 1-6, California Institute of Technology, Pasadena

Table 5. Observed model-free photometric data in B and colour characteristics

Galaxy	R.A. (1950) [^{h} ^{m} ^{s}]	Decl. [^{o} $'$ $''$]	B_T [^{m}]	B_{25} [^{m}]	r_{25} [$''$]	b/a	PA [^{o}]	$\mu_{B,0}$ [$^m/\Box''$]	$r_{\rm eff}$ [$''$]	$(B-R)_0$ [^{m}]	B_T-R_T [^{m}]	$\frac{\Delta(B-R)}{\Delta r}$ [$^m/''$]	$\pm\ \sigma$
(1)	(2)	(3)	(4)	(5)	(6)	(7)	(8)	(9)	(10)	(11)	(12)	(13)	
VN2#451	10 40 15	-00 11 00	18.59	18.78	5.7	0.51	104	22.1	2.9	1.5	1.24	-0.091	.006
VN2#426	10 40 34	00 10 05	17.49	17.61	9.3	0.48	76	21.7	4.0	1.5	0.93	-0.017	.005
VN2#417	10 40 36	-00 02 06	18.14	18.32	6.3	1		21.8	3.2	1.3	1.10	-0.029	.009
VN2#420	10 40 37	00 14 51	18.75	18.97	5.4	0.90	44	22.3	3.3	1.7	1.33	-0.072	.009
VN2#421	10 40 37	00 17 46	17.35	17.50	8.9	0.72	122	21.35	4.4	1.6	1.35		
VN2#381	10 40 57	-00 19 18	18.55	18.80	6.0	0.67	53	23.0	3.9	1.2	1.13		
VN2#378	10 41 00	-00 05 30	18.03	18.15	6.8	0.57	96	20.9	2.0	2.4	1.70		
VN2#377	10 41 04	-00 04 26	18.62	18.77	8.4	0.62	40	22.8	4.1	1.9	1.40	-0.033	.004
VN2#K627	10 41 12	-00 09 38	16.14	16.27	13.3	0.67	154	19.5	3.4	1.9	1.41		
VN2#361	10 41 13	-00 07 25	19.28	19.64	5.3	0.36	151	23.2	3.8	1.6	1.27	-0.064	.006
VN2#341	10 41 23	-00 03 20	18.93	19.10	5.1	0.57	43	22.6	3.1	1.6	1.43	-0.055	.007
VN2#302	10 41 43	00 17 24	17.14	17.31	10	1		21.9	7.0	1.5	1.32		
VN2#291	10 41 56	00 14 16	18.48	18.71	6.2	0.82	3	22.5	3.6	1.3	0.98		
VN2#K456	10 41 55	00 00 59	19.42	19.92	4.7	1		23.9	3.8	1.3	1.20	-0.020	.009
VN2#274	10 42 08	-00 00 18	18.54	18.91	5.8	0.46	139	23.05	4.0	1.1	0.50	-0.033	.006
VN2#K363	10 42 10	00 04 07	17.72	18.51	8.9	0.70	170	23.0	9.1	1.2	1.00	-0.011	.003
VN2#232	10 42 29	-00 15 19	19.37	19.62	4.0	0.77	169	23.1	2.6	1.6	1.44		
VN2#203	10 42 48	-00 04 29	18.28	18.49	6.4	0.78	4	22.95	3.8	2.0	1.38	-0.106	.007
VN2#K213	10 42 50	-00 04 52	17.96	18.07	8.3	0.65	44	23.2	6.4	2.2	1.14		
VN2#188	10 42 57	00 00 18	17.03	17.36	10.9	0.76	148	20.5	5.0	1.4	1.83		
VN2#187	10 43 01	-00 09 46	17.84	17.99	5.6	0.42	92	21.5	2.7	1.4	1.34		
VN2#K117	10 43 23	-00 10 36	18.50	19.36	4.8	1		23.0	6.3	0.8	0.88		
VN2#136	10 43 52	00 16 28	18.26	18.56	6.9	0.45	169	22.4	4.3	1.2	0.99		
1021+0024	10 21 36	00 24 00	15.85	15.92	11.5	0.61	167	18.8:	3.0				
1022-0036	10 22 00	-00 36 00	15.60	15.65	18.2	0.65	165	19.8	6.5				
O0467-074	10 32 50	-01 21 42	17.22	17.67	11.5	0.97	34	23.0	8.6	1.0	0.83	-0.015	.006
O0467-023	10 33 36	00 37 54	18.35	19.18	6.4	0.45	64	23.1	6.6	0.8	0.46:	-0.026	.006
HN1296	10 50 45	01 19 24	16.33	16.44	12.0	0.61	10:	21.3	6.1	1.3	0.84		
VN4#217	13 03 42	34 09 05	18.49	18.67	5.3	0.80	52	22.0	3.0	1.8	1.56		
VN4#211	13 03 44	34 04 06	19.05	19.38	4.7	0.88	26	22.9	3.1	0.9	0.86		
VN4#198	13 04 08	33 55 04	18.06	18.44	8.0	0.90	59	23.4	5.8	1.5	1.06	-0.033	.004
VN4#197	13 04 13	33 52 06	18.82	19.04	4.5	0.86	110	22.4	2.6	1.4	1.12	-0.056	.011
VN4#186	13 04 22	34 10 19	19.45	20.03	4.3	0.68	14	23.7	3.5	1.2	1.05	-0.068	.006
VN4#177	13 04 33	34 09 59	18.26	18.44	5.4	0.91	143	22.1	2.8	1.6	1.38	-0.047	.006
VN4#158	13 04 50	34 02 30	17.52	17.77	8.3	0.34	0	22.25	4.6	1.4	1.12		
VN4#134	13 05 21	34 02 36	19.04	19.46	4.8	0.64	99	23.3	3.7	1.3	1.22		
VN4#122	13 05 36	34 04 20	20.21	20.78	2.9	0.56	158	23.85	2.5	1.8	1.06	-0.180	.024
VN4#109	13 05 44	34 22 46	18.14	18.52	6.9	0.56	13	22.35	4.5	1.3	1.34	-0.006	.002
VN4#119N	13 05 47	33 45 10	18.28	18.55	6.2	0.54	155	22.45	3.9	0.8	0.78		
VN4#148	13 05 02	34 15 40	18.53	18.91	5.8	0.65	105	22.9	3.9	1.8	1.63		
VN4#156	13 05 01	34 16 40	17.96	18.40	6.9	0.77	83	21.9	3.8	2.0	1.67	-0.051	.003
VN4#80	13 06 24	34 10 35	18.07	18.27	7.2	0.81	20	22.6	4.1	1.0	1.05		
VN4#71	13 06 39	34 05 13	18.45	18.95	5.8	0.89	93	22.5	4.5	1.5	1.01	-0.073	.005
VN4#71N	13 08 01	34 15 58	17.56	17.82	9.0	0.31	61	22.6	5.4	1.5	1.30	-0.032	.004
VN4#54	13 07 08	33 44 38	19.10	19.62	4.5	0.75	105	23.15	3.6	2.1	1.78	-0.036	.006
VN4#40	13 07 35	33 52 30	18.03	18.17	6.7	0.93	55	22.35	3.7	1.2	1.00		
VN4#32	13 07 40	33 52 52	19.26	19.57	4.1	0.50	113	22.8	2.7	1.1	1.26		
1305+3416	13 05 34	34 21 13	15.31	15.52	17.2	0.80	71	19.2	5.0	1.5	1.48		
1305+3421	13 05 43	34 16 27	15.10	15.17	17.3	0.80	67	19.6	6.1	1.5	1.40		
UGC 8227	13 06 15	34 14 31	15.10	15.18	18.7	0.30	77	19.9	7.3	1.7	1.55	-0.004	.001

Table 5. continued

(1)	(2)	(3)	(4)	(5)	(6)	(7)	(8)	(9)	(10)	(11)	(12)	(13)	
B609–034	00 38 44	12 12 18	18.77	19.62	5.6	0.67	30	24.1	5.9	1.2	1.00		
O0010–019	00 05 20	11 35 06	16.45	17.15	16.5	0.81	124	22.7	10.2	1.6	1.27		
O0010–113	00 01 26	14 25 48	16.90	17.06	12.7	0.72	150	22.1	7.6				
O0319–117	00 07 59	01 14 30	17.60	18.25	8.1	0.79	150	22.5	7.3				
O0319–157	00 11 34	00 54 12	17.07	17.27	10.6	0.53	8	22.15	6.1				
O0591–013	00 17 11	00 05 06	17.84	18.13	8.1	0.56	117	22.4	5.1				
O0591–043	00 25 06	00 14 36	15.90	15.99	14.8	0.86	7	21.05	7.2				
O0823–020	00 26 34	13 30 18	18.83		3.2	0.64	114	24.6	7.9	1.5	1.21		
O0823–055	00 35 13	11 32 18	18.49	19.26	6.7	0.61	26	24.1	6.8	1.2	1.03		
O1274–017	00 54 08	13 57 06	17.88	18.13	8.1	0.58	15	23.2	5.2	1.2	1.00		
O1274–032	00 46 52	12 16 00	16.30	16.48	15.3	0.70	176	21.35	8.3				
VN8#002	00 28 55	09 47 40	17.90	18.22	7.0	0.27	11	22.4	4.0	0.8	0.70	-0.014	.004
VN8#003	00 29 36	09 52 43	16.42	16.49	10.2	0.90	40	19.6	2.8	1.1	0.96		
VN8#004	00 29 36	09 53 07	18.57	18.75	5.3	0.57	168	22.5	3.0	1.5	1.16		
VN8#005	00 58 23	19 51 09	18.80	19.55	5.3	0.67	68	22.7	3.2	1.6	0.97		
VN8#007	00 58 37	19 38 33	17.77	18.10	8.8	0.75	0	22.4	5.4	1.5	1.18	-0.035	.007
VN8#008	00 58 44	19 50 31	17.90	18.05	5.3	0.75	170	20.4	2.7	1.1	1.48	0.041	.006
VN8#009	00 58 45	10 08 33	19.45	19.65	4.2	0.46	170	22.7	2.9	1.4	0.64		
VN8#010	00 58 48	19 56 26	17.50	17.52	8.4	0.50	75	22.0	4.1	2.4	1.48	-0.087	.004
VN8#011	00 59 13	19 46 42	17.21	17.35	9.6	0.80	110	21.8	5.0	1.7	1.07	-0.064	.005
VN8#012	00 59 19	20 19 52	18.14	18.30	6.7	0.27	70	22.4	3.8	1.8	1.35	-0.032	.006
VN8#013	00 59 23	20 18 39	19.60	21.14	2.1	0.70	105	23.0	6.6	2.5	1.60		
VN8#014	00 59 26	20 18 46	18.42	18.57	7.3	0.60	80	22.8	3.3	1.5	1.44	-0.037	.005
VN8#015	00 59 43	19 36 54	17.85	17.85	7.4	0.82	110	21.3	3.1	1.3	1.05		
VN8#016	00 59 47	09 44 27	18.44	18.64	5.3	0.77	70	21.2	2.6	0.6	0.46		
VN8#017	01 00 40	19 38 10	18.86	18.94	4.5	0.77	65	21.7	2.8	1.3	1.03		
VN8#018	01 00 50	19 44 11	18.38	18.82	5.5	0.72	150	21.5	3.6	2.5	1.84		
VN8#019	01 01 13	10 19 21	15.45	15.74	17.6	0.80	70	20.3	7.0	1.8	1.62		
VN8#020	01 01 28	10 18 46	18.80	19.10	5.8	0.35	95	22.5	3.8	1.7	1.13	-0.071	.006
VN8#021	01 01 37	19 54 04	18.22	18.40	6.5	0.92	20	22.1	3.9	2.2	1.42		
UGC 32	00 02 25	11 25 23	15.80	16.34	17.5	0.80	79	22.1	13.3	2.0	1.78		
2357+0051	23 57 40	00 50 31	15.04	15.08	20.5	0.74	147	21.0	10.0				

Table 6. Observed model-free photometric data in R

Galaxy	R.A. (1950) [^{h} ^{m} ^{s}]	Decl. [^{o} $'$ $''$]	R_T [^{m}]	R_{25} [^{m}]	r_{25} [$''$]	b/a	PA [^{o}]	$\mu_{R,0}$ [$^m/\Box''$]	$r_{\rm eff}$ [$''$]
(1)	(2)	(3)	(4)	(5)	(6)	(7)	(8)	(9)	(10)
VN4#163	13 04 52	33 55 42	18.6	19.2	5.3	0.68	138	22.8	4.2
O0467-087	10 27 27	-01 26 42	16.35	16.38	11.8	0.66	165:	21.0	5.0
O0991-008	10 44 36	-05 09 00	17.15	17.30	9.6	0.79	73	21.8	5.4
O0010–044	00 05 10	12 46 06	17.94	18.15	8.3	0.78	132	22.8	5.3
O0010–055	23 58 16	12 30 12	18.02	18.53	7.9	0.57	164	23.3	6.4
O0823–006	00 31 44	14 24 42	17.73	17.83	8.1	0.83	9	21.9	4.3
O0823–109	00 21 56	14 08 06	15.70	15.75	14.9	0.89	89	20.2	6.5
O0823–113	00 21 02	14 48 12	17.33	17.63	10.4	0.74	6	22.4	6.8
O1274–006	00 50 22	14 59 18	16.98	17.07	9.4	0.84	34	21.2	4.2
O1274–037	00 54 29	12 11 24	17.41	17.52	8.9	0.77	72	21.5	4.4

Table 7. Reduced photometric data and exponential model parameters in B

Galaxy	D	M_B	$r_{\rm eff}$	$\mu^{\rm c}_{\rm eff}$	α^{-1}		$\mu_0^{\rm exp}$	$\mu_{0,\rm c}^{\rm exp}$	n	profile type	isol. class
	[Mpc]	[^{m}]	[kpc]	[$^m/\Box''$]	[$''$]	[kpc]	[$^m/\Box''$]				
(1)	(2)	(3)	(4)	(5)	(6)	(7)	(8)	(9)	(10)	(11)	(12)
VN2#451	341.7	-19.14	4.8	22.90	2.2	3.9	21.62	22.09	1.0	d	
VN2#426	247.2	-19.54	4.8	22.49	5.4	7.0	22.16	22.70	1.1	bdd	
VN2#417	365.7	-19.74	5.7	22.67	1.6	3.0	21.40	21.16	1.0	d	
VN2#420	500.4	-19.81	8.0	23.34	1.7	4.5	22.20	22.05	1.0	d:	
VN2#421	330.3	-20.30	7.1	22.58	2.6	4.5	21.30	21.40	1.3	d	
VN2#381	72.9	-15.82	1.4	23.48	2.2	0.9	22.05	22.22	1.4:	cd:h:	2
VN2#378	292.8	-19.36	2.9	21.56	1.5:	2.7	21.1:	21.4:	1.9	dc	
VN2#377	241.2	-18.35	4.7	23.67	2.1	4.5	21.64	21.90	0.6	dd	
VN2#K627	157.0	-19.90	2.6	20.83					4	bd	2
VN2#361				24.15	1.8		22.28	23.13	1.0	c:d	
VN2#341	489.9	-19.58	7.4	23.39	1.7	4.5	22.04	22.39	1.0:	dd	
VN2#302	267.1	-20.05	9.1	23.37	2.4	3.3	21.51	21.25	0.8	d:	
VN2#291	376.7	-19.46	6.6	23.28	2.2	4.4	22.26	22.22	0.8	dc	
VN2#K456	151.8	-16.55	2.8	24.32	1.7	1.4	22.95	22.69	1.0	cd	1
VN2#274	114.8	-16.82	2.2	23.58	2.4	1.4	21.94	22.52	0.9	cd	2
VN2#K363	61.9	-16.30	2.7	24.53	4.4	1.4	22.75	22.88	1.7	d	3
VN2#232	1012.5	-20.72	12.8	23.80	1.0	4.9	20.87	20.89	0.6:	cd	
VN2#203	597.7	-20.66	11.1	23.21	1.8	5.5	21.71	21.72	0.7	cdc:	
VN2#K213	104.2	-17.19	3.3	23.91	3.7	1.9	22.90	23.11	1.0	cdc:	3
VN2#188	158.1	-19.02	3.8	22.52					4	bd	2
VN2#187	344.2	-19.90	4.5	21.99	1.6	2.9	20.00	20.68	0.9	dd	
VN2#K117	68.6	-15.74	2.1	24.50	3.9	1.4	23.96	23.70	3	bd	3
VN2#136	154.7	-17.75	3.2	23.42	3.1	2.6	22.05	22.65	1.1	d	2
1021+0024	95.3	-19.11	1.4	20.18	2.0	1.0	19.82	20.23	1.9	bdh:	6
1022-0036	135.4	-20.12	4.3	21.60	4.8	3.4	21.21	21.79	1.2:	bd	5
O0467-074	96.5	-17.76	4.0	23.83	5.6	2.8	22.95	22.90	0.8	dc:	6
O0467-023	141.6	-17.46	4.5	24.39	4.7	3.5	23.65	24.14	1.5	bd	5
HN1296	148.3	-19.59	4.4	22.20	3.2	2.5	21.07	21.40	0.9	d:	4
VN4#217	495.0	-20.00	7.3	22.87	1.4	3.6	20.86	20.84	1.1	d	
VN4#211	309.5	-18.43	4.7	23.52	1.5	2.4	21.83	21.77	0.6	c:dh:	
VN4#198	148.0	-17.85	4.3	23.87	2.9	2.4	22.57	22.48	0.7	d:d	2
VN4#197	867.2	-20.88	11.0	22.89	1.1	5.1	21.00	20.95	1.8	cd:h	
VN4#186	316.4	-18.08	5.4	24.13	1.5	2.5	22.27	22.49	0.7	cd	
VN4#177	496.8	-20.24	6.9	22.51	1.2	3.1	20.48	20.38	1.2	cd:h:	
VN4#158	138.0	-18.25	3.2	22.83	2.3	1.7	21.37	22.34	0.8	d	1
VN4#134	132.0	-16.63	2.4	23.88	1.8	1.3	22.42	22.64	0.9	dh:	1
VN4#122	413.8	-17.90	5.1	24.20	1.2	2.5	22.92	23.35	1.4	d	
VN4#109	130.4	-17.51	3.0	23.42	2.6	1.8	22.15	22.58	0.9	dh:	1
VN4#119N	205.9	-18.33	4.0	23.23	2.0	2.2	21.96	22.43	1.0	d	
VN4#148	138.8	-17.25	2.7	23.48	2.3	1.7	22.36	22.63	2.0	bd:	1
VN4#156	396.0	-20.05	7.4	22.85	2.1	4.4	21.66	21.74	0.9	dh:	
VN4#080	131.6	-17.60	2.7	23.13	2.1	1.5	21.67	21.70	0.8	cd	1
VN4#071	259.2	-18.65	5.7	23.71	2.7	3.8	22.95	22.88	2.0	bd	1
VN4#071N	135.6	-18.17	3.7	23.22	2.7	2.0	21.78	22.85	0.7	dd	
VN4#054	738.8	-20.26	12.8	23.85	1.9	7.3	22.29	22.40	1.2	d	
VN4#040	345.2	-19.69	6.3	22.88	1.5	2.8	20.93	20.81	0.7	d:d	
VN4#032	345.2	-18.46	4.6	23.41	1.2	2.3	21.78	22.33	1.3	cd:	
1305+3416	132.8	-20.37	3.3	20.80					24:	bd:	1
1305+3421	134.4	-20.61	4.1	21.02	3.6	2.6	20.00	20.04	1.2	bdh	1
UGC 8227	135.6	-20.63	4.9	21.41	4.0	2.9	19.99	20.87	0.8	bpec	1

Table 7. continued

(1)	(2)	(3)	(4)	(5)	(6)	(7)	(8)	(9)	(10)	(11)	(12)
B609–034	149.4	-17.27	4.3	24.45	3.5	2.7	23.49	23.65	0.8	cd	2
O0010-019				23.32	5.3		22.13	22.09	0.5	dc	
O0010-113	368.5	-21.10	13.6	23.13	5.9	11.3	22.50	22.59	0.7	bdd	
O0319-117	155.2	-18.52	5.5	23.75	3.8	3.2	22.75	22.74	1.6	bd	2
O0319-157	158.3	-19.10	4.7	22.83	3.1	2.6	21.72	22.14	0.8	b:d	2
O0591-013	163.2	-18.39	4.0	23.21	3.0	2.6	22.33	22.69	1.0	dc:	2
O0591-043	239.1	-21.16	8.3	22.02	3.1	4.0	20.25	20.14	1.2	cd	
O0823-020				25.15	4.6		24.23	24.44	0.8	d	
O0823-055	123.6	-17.14	4.1	24.48	3.8	2.3	23.44	23.71	0.5	cd:	6
O1274-017	138.3	-17.99	3.5	23.29	2.4	1.7	21.66	21.98	0.6	cd	5
O1274-032	148.5	-19.73	6.0	22.73	4.8	3.7	21.79	21.91	0.8	b:d	2
VN8#002	62.6	-16.25	1.2	22.74	1.9	0.6	21.34	22.50	0.9	c:d	2
VN8#003	154.8	-19.70	2.1	20.49	2.4	2.0	20.90	20.75	1.5	bd	3
VN8#004	534.5	-20.24	7.8	22.79	1.4	3.8	21.2:	21.5:	0.7	cd:	
VN8#005	348.1	-19.08	5.5	23.18	1.7	3.1	22.2	22.36	0.8	d:d	
VN8#007	237.3	-19.28	6.3	23.28	3.1	3.8	22.34	22.38	1.0	dc:	
VN8#008	457.5	-20.57	5.9	21.85	3.6	8.7	23.1:	23.2:	3	I bd	
VN8#009	594.1	-19.59	8.3	23.57	1.3	4.0	22.14	22.71	1.0	d:d	
VN8#010	253.2	-19.69	5.1	22.40	1.6	2.1	21.2:	21.7:	0.6	b:d	
VN8#011	255.9	-20.00	6.2	22.53	2.4	3.3	21.4:	21.4:	0.8	dc:	
VN8#012	445.9	-20.28	8.2	22.87	4.9	11.5	24.8:	25.9:	0.7:	bdc	
VN8#013	741.0	-19.92	23.7:						6	bd:	
VN8#014	615.3	-20.70	9.7	22.81	2.1	6.8	21.84	22.12	1.0	c:dh:	
VN8#015	253.3	-19.34	3.8	22.16	2.0	2.6	21.32	21.27	1.0	d	
VN8#016	213.5	-18.38	2.7	22.38	1.6	1.8	21.8	21.8	1.3	bd	
VN8#017	454.6	-19.60	6.1	22.90	1.3	3.0	21.56	21.57	1.0	d	
VN8#018	708.1	-21.04	12.5	23.01	3.1	11.7	23.0:	23.1:	3:	bd	
VN8#019	154.1	-20.71	5.3	21.49					7		3
VN8#020	227.3	-18.15	4.2	23.53	1.9:	2.3	22.2:	23.1:	0.9	c:dc	
VN8#021	461.9	-20.27	8.6	22.98	1.6:	3.6:	20.8:	20.6:	0.7	d:dh:	
UGC 32	303.2	-21.78	19.5	23.25	7.7	12.3	22.40	22.37	1.8		
2357+0051	100.0	-20.13	4.8	21.87	4.8	2.5	20.62	20.68	0.7	d:	3

Table 8. Reduced photometric data and exponential model parameters in R

Galaxy	D	M_R	$r_{\rm eff}$	$\mu^{\rm c}_{\rm eff}$	α^{-1}		$\mu_0^{\rm exp}$	$\mu_{0,\rm c}^{\rm exp}$	n	profile type	isol. class
	[Mpc]	[^{m}]	[kpc]	[$^m/\Box\,''$]	[$''$]	[kpc]	[$^m/\Box\,''$]				
(1)	(2)	(3)	(4)	(5)	(6)	(7)	(8)	(9)	(10)	(11)	(12)
VN4#163	204.3	-18.00	4.1	23.63	2.4	2.4	22.74	23.06	1.9	d:	
O0467-087	133.8	-19.28	5.0	21.85	3.1	2.2	20.82	21.01	1.1	dc	5
O0991-008	150.7	-18.74	5.4	22.82	3.1	2.4	21.69	21.85	0.8	d:c	1
O0010–044	152.4	-18.12	3.9	23.41	3.0	2.2	22.38	22.50	0.6	dd	2
O0010–055	64.1	-16.16	2.0	24.05	3.9	1.2	23.02	23.48	0.9	d	4
O0823–006	145.3	-18.23	3.0	22.75	2.6	1.9	21.84	21.89	1.0	d	2
O0823–109	165.5	-20.54	5.2	21.76	3.4	2.7	20.47	20.45	1.0	bdd	2
O0823–113	67.3	-16.96	2.2	23.34	4.0	1.3	22.39	22.57	1.1	b:d	2
O1274–006	492.5	-21.63	10.0	21.95	2.4	5.7	20.95	20.99	1.1	d	
O1274–037	162.4	-18.79	3.5	22.48	2.5	2.0	21.47	21.60	1.0	bdc	3

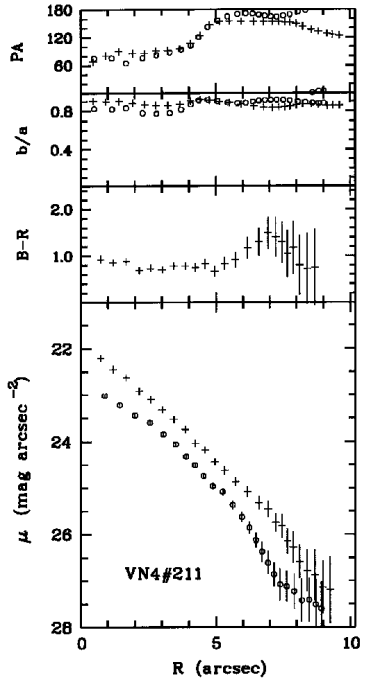

Fig. 10. The same as Fig. 9 for VN4#211; B profile is of type **cdh:** (RB94) or V (BC91), R profile is of type **c:dh:** (RB94) or IV-V (BC91)

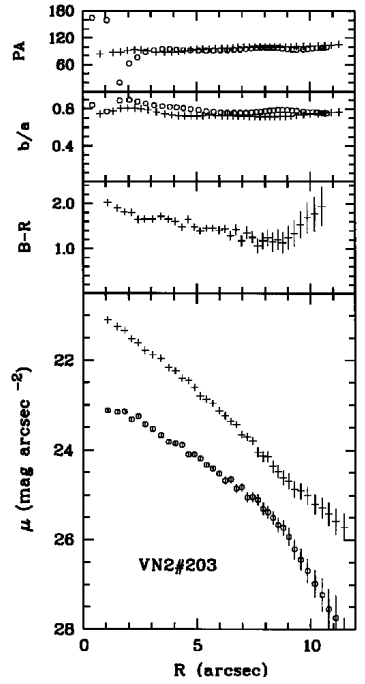

Fig. 11. The same as Fig. 9 for VN2#203; B profile is of type **cdc** (RB94) or V (BC91), R profile is of type **d** (RB94) or IV (BC91)

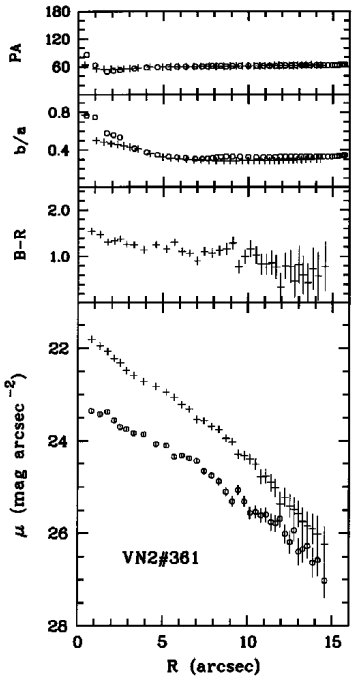

Fig. 12. The same as Fig. 9 for VN2#361; B profile is of type **c:d** (RB94) or IV-V (BC91), R- profile is of type **dc:** (RB94) or IV-V (BC91)

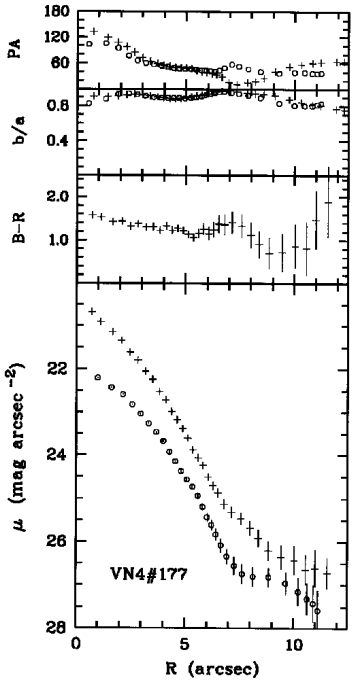

Fig. 13. The same as Fig. 9 for VN4#177; B and R profiles are both of type **cd:h** (RB94) or V: (BC91)

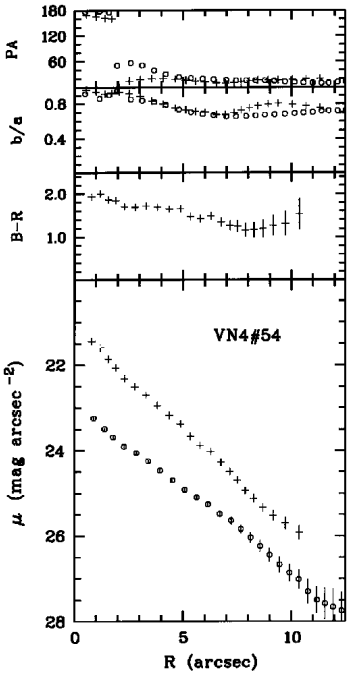

Fig. 14. The same as Fig. 9 for VN4#54; B and R profiles are both of type **d** (RB94) or IV (BC91)

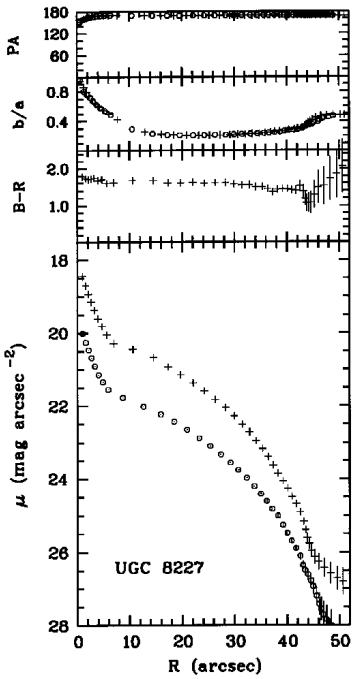

Fig. 16. The same as Fig. 9 for UGC 8227; B and R profiles are both of specific multicomponental type – **bpec** (RB94) or IIIpec (BC91) with prominent "bulge" component and untypical for disk-galaxies convex curvature over linear radius

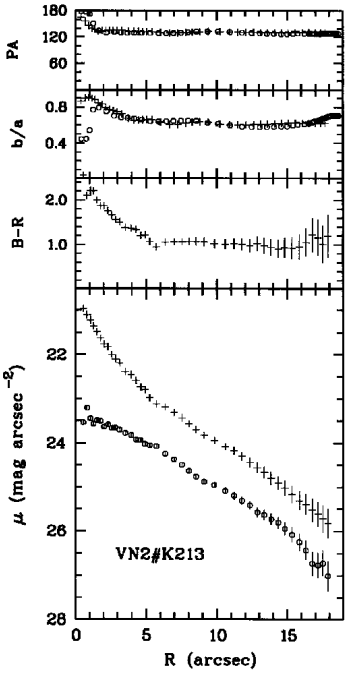

Fig. 15. The same as Fig. 9 for VN2#K213; B profile is of type **cdc:** (RB94) or IV-V (BC91), R profile is of type **bd** (RB94) or IIIa (BC91)

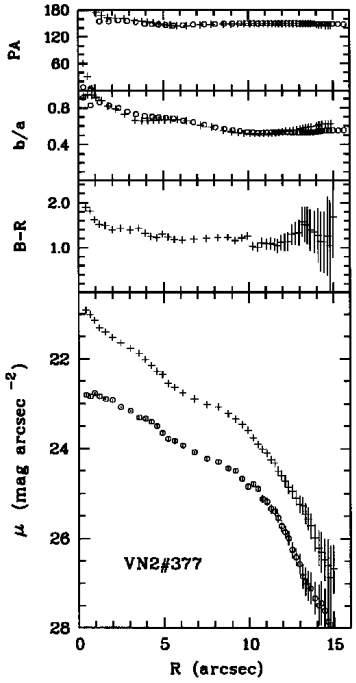

Fig. 17. The same as Fig. 9 for VN2#377; B and R profiles both show two disk components, the internal disk having larger scale length - type **dd:** (RB94) or IIIpec (BC91)

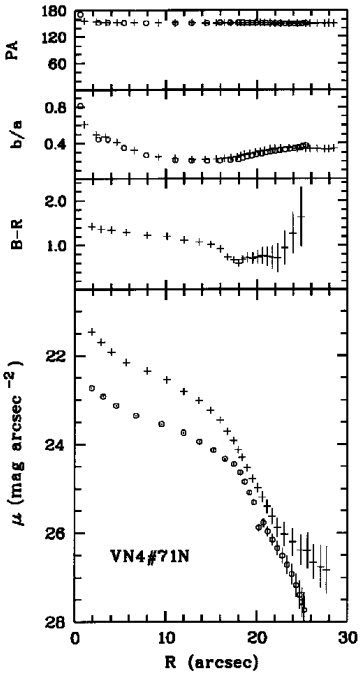

Fig. 18. The same as Fig. 9 for VN4#71N; B and R profiles are both of type **dd** (RB94) or IIIpec (BC91)

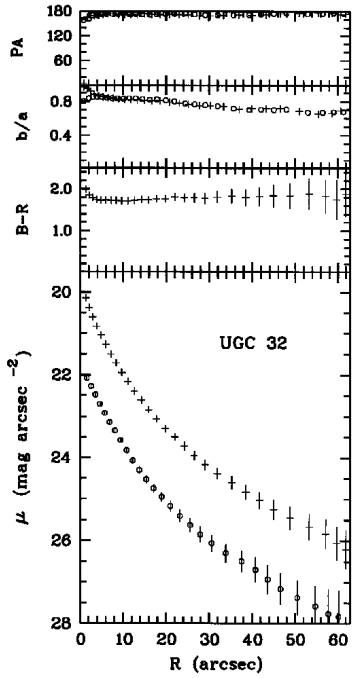

Fig. 19. The same as Fig. 9 for UGC 32; profile type I (BC91)